BIOCHEMISTRY
including biophysical chemistry & molecular biology

Article

pubs.acs.org/biochemistry

Structural and Biochemical Characterization of Human Adenylosuccinate Lyase (ADSL) and the R303C ADSL Deficiency-Associated Mutation

Stephen P. Ray,[†,‡] Michelle K. Deaton,[‡,§] Glenn C. Capodagli,[‡,§] Lauren A. F. Calkins,[§] Lucas Sawle,[†] Kingshuk Ghosh,[†,‡] David Patterson,*[,‡,∥] and Scott D. Pegan*[,‡,§]

[†]Department of Physics and Astronomy, [‡]Eleanor Roosevelt Institute, [§]Department of Chemistry and Biochemistry, and [∥]Department of Biological Sciences, University of Denver, Denver, Colorado 80208-0183, United States

Supporting Information

ABSTRACT: Adenylosuccinate lyase (ADSL) deficiency is a rare autosomal recessive disorder, which causes a defect in purine metabolism resulting in neurological and physiological symptoms. ADSL executes two nonsequential steps in the de novo synthesis of AMP: the conversion of phosphoribosylsuccinyl-aminoimidazole carboxamide (SAICAR) to phosphoribosylaminoimidazole carboxamide, which occurs in the de novo synthesis of IMP, and the conversion of adenylosuccinate to AMP, which occurs in the de novo synthesis of AMP and also in the purine nucleotide cycle, using the same active site. Mutation of ADSL's arginine 303 to a cysteine is known to lead to ADSL deficiency. Interestingly, unlike other mutations leading to ADSL deficiency, the R303C mutation has been suggested to more significantly affect the enzyme's ability to catalyze the conversion of succinyladenosine monophosphate than that of SAICAR to their respective products. To better understand the causation of disease due to the R303C mutation, as well as to gain insights into why the R303C mutation potentially has a disproportional decrease in activity toward its substrates, the wild type (WT) and the R303C mutant of ADSL were investigated enzymatically and thermodynamically. Additionally, the X-ray structures of ADSL in its apo form as well as with the R303C mutation were elucidated, providing insight into ADSL's cooperativity. By utilizing this information, a model for the interaction between ADSL and SAICAR is proposed.

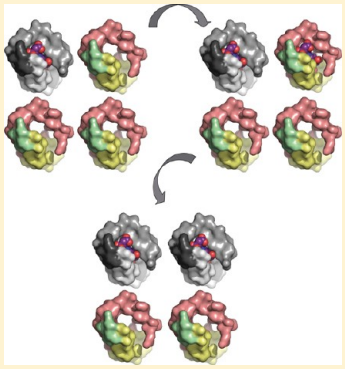

Adenylosuccinate lyase (ADSL) deficiency is a rare autosomal recessive disorder characterized by serious neurological and physiological symptoms such as psychomotor retardation (PMR), expression of autistic features, structural brain abnormalities, axial hypotonia, seizures, peripheral hypotonicity, ataxia, muscle wasting, growth retardation, and strabismus.[1−3] More than 60 cases of ADSL deficiency have been reported worldwide, but it is widely considered to be underdiagnosed.[4−6] ADSL deficiency is clinically diagnosed by elevated levels of succinylaminoimidazolecarboxamide riboside (SAICAr) and succinyladenosine (S-Ado) in urine, plasma, and cerebrospinal fluid.[7] Three distinct phenotypic groups have been established: (1) neonatal, (2) type I and (3) type II. The neonatal form results in fatal neonatal encephalopathy and has an S-Ado:SAICAr ratio of <1. Type I patients experience early onset, severe PMR and have a ratio of ∼1. Type II patients experience later onset with mild PMR and have a ratio of 2−4.[8] There are three main hypotheses that describe the difference in ratio: (1) nonparallel reduction in the enzyme's activity on its substrates, (2) differential dephosphorylation or transport of the substrates out of the cells,[9,10] and (3) inability of the ADSL mutant protein to form an active purinosome, which is formed when purine synthesis is required and is needed for appropriate channeling of SAICAR through the de novo purine synthesis pathway.[11]

ADSL conducts two nonsequential steps of de novo AMP synthesis, the conversion of succinylaminoimidazolecarboxamide ribonucleotide (SAICAR) and succinyladenosine monophosphate (SAMP) into aminoimidazolecarboxamide ribotide (AICAR) and adenosine monophosphate (AMP), respectively, with the concomitant release of fumarate in each case.[12] The conversion of SAMP to AMP is also part of the purine nucleotide cycle. So far, all mutations, with one exception, result in a proportional loss of enzyme activity with the two substrates. The ADSL carrying the R303C mutation has been observed as a homozygous mutation in two unrelated patients. It is a type II mutation and results in the mildest observed form of ADSL deficiency. Interestingly, this mutation shows a more severe loss of activity with SAMP than with SAICAR, although the extent of disproportionality varies from study to study, perhaps reflecting differences in how the enzyme assays were conducted. Some investigators were unable to detect activity with SAMP in extracts from fibroblasts,[13] while others found 3% of normal activity.[8] In other cases using different recombinant ADSL constructs, 7 and 18% of wild-type (WT)

Received: June 15, 2012
Revised: July 18, 2012
Published: July 19, 2012

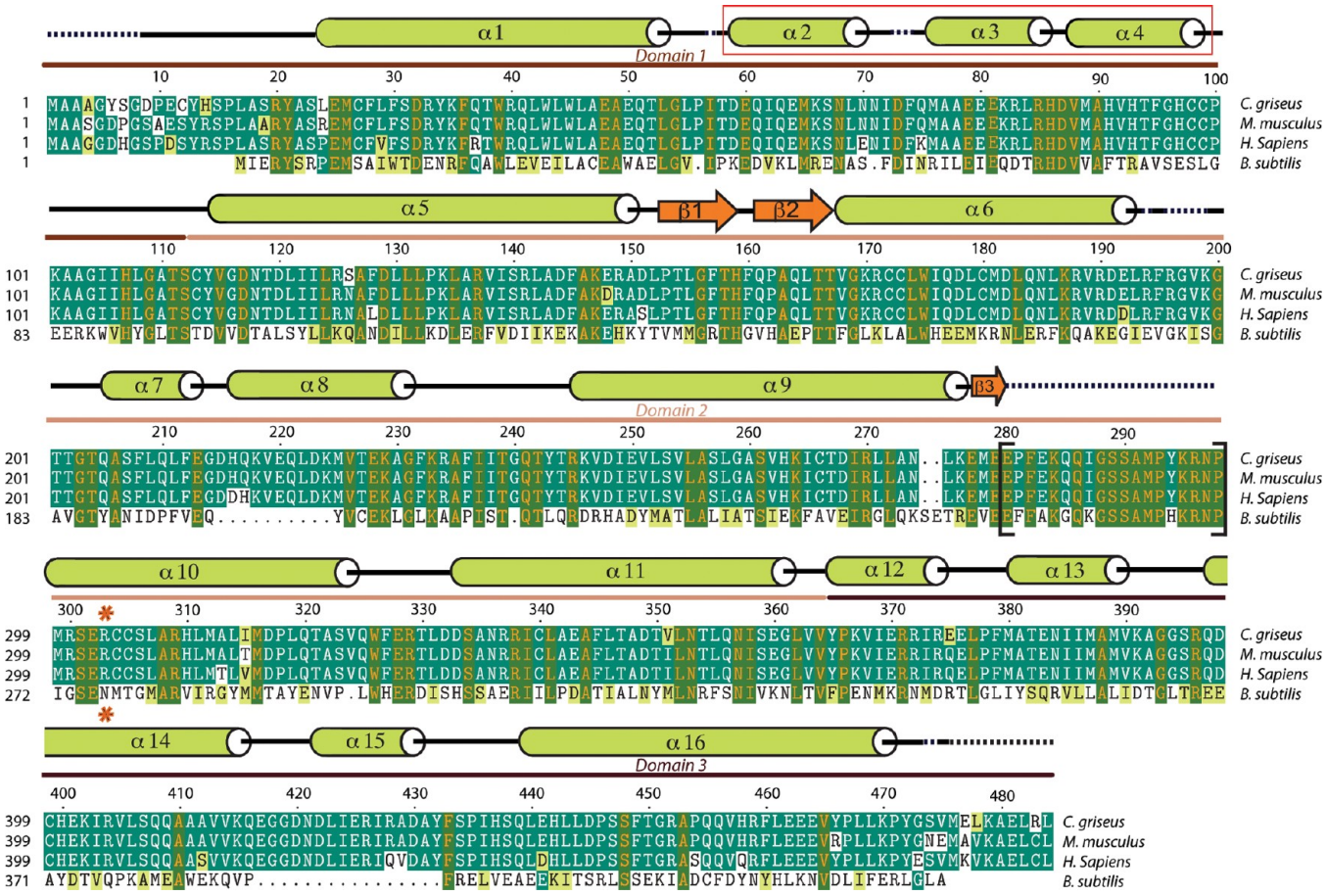

Figure 1. Sequence alignment of ADSL from various species. ADSLs are from *H. sapiens* (GenBank entry AAC83935.1), *Mus musculus* (GenBank entry AAB60684.1), *B. subtilis* (NCBI Reference Sequence YP_003865018.1), and *Cricetulus griseus* (NCBI Reference Sequence NP_001230974.1). The secondary structure of hADSL according to Defined Secondary Structure of Proteins (DSSP) is represented by green cylinders (helical regions), orange arrows (β-sheet regions), black lines (loops), and black dashes (unstructured regions). Mutation site 303 is marked with an asterisk. The location of helices α3 and α4 is highlighted with a red box. The C3 loop is enclosed in brackets. Catalytic residues H159 and S289 are marked with blue asterisks. Domains 1−3 are indicated with bars in shades of brown.

activity were observed with SAMP and 44% was observed with SAICAR.[13,14] The reason for the nonparallel loss of activity is not yet understood, nor is the reason why this mutation leads to such a mild phenotype. Hypotheses include the possibility that different amino acids in the active site bind the two substrates, that cysteine is not able to interact well with SAMP, and that there are alterations in the stability of the active site cleft.[13,14]

Crystal structures of the bacterial ADSL and other studies have provided insight into the active site and the catalytic mechanism; however, these studies predominately use bacterial ADSL from organisms such as *Thermotoga maritima* or *Escherichia coli*.[15,16] *T. maritima* and *Homo sapiens* have a level of sequence identity of 25% and a level of similarity of 57%. *E. coli* and *H. sapiens* have a level of sequence identity of 23% and a level of similarity of 57%. ADSL was found in these bacterial species to function in the pathway as a homotetramer (Figure 1). Interestingly, three monomers contribute to each of the four active sites in the tetramer.[9,17] The use of *Bacillus subtilis* ADSL in particular as a model to study the properties of mutant enzymes in some cases involved modification of additional amino acid residues in the *B. subtilis* ADSL to make it more closely resemble human ADSL.[18,19] However, attempts to make use of a *B. subtilis* model system to replicate the R303C phenomenon have proven to be difficult because *B. subtilis* and *H. sapiens* have a level of sequence identity of only 30% and a level of similarity of 63%. Specifically, the sequence diversity of *B. subtilis* and *H. sapiens* results in multiple alterations within the active site, including, but not limited to, an asparagine residue in place of the corresponding R303 in human ADSL, as well as an arginine residue in place of the corresponding T354 in human ADSL. Not surprisingly, the removal of *B. subtilis*'s asparagines at the corresponding human ADSL R303 position for cysteine did not generate a disproportional reduction in catalytic ability.[18,19] This observation as well as others suggests that the study of the bacterial enzyme, while initially useful for understanding some of the basic features of ADSL, such as its tetrameric nature and the participation of three subunits in forming each active site, may not be as useful for understanding the effects of various disease-causing mutations on the human enzyme. Only limited structural information about the human ADSL active site in the unpublished SAMP-bound and S-AMP/AMP-fumarate-bound PDB deposited entries [Protein Data Bank (PDB) 2J91 and 2VD6] exists. Current studies of disease-associated mutations of human ADSL have focused on the correlation of substrate activity with clinical phenotypes, the thermal stability of ADSL, the activity of hybrid WT ADSL and mutants, and global changes in structure.[14,20−23] They have not investigated local structural changes or properties of the

dx.doi.org/10.1021/bi300796y | *Biochemistry* 2012, 51, 6701−6713

binding to the products within the ADSL active site. In this study, we present structural and biochemical characterization data of WT and mutant R303C ADSL by enzyme kinetics, product binding by isothermal titration calorimetry (ITC), and X-ray crystallography to reveal the effects of the R303C mutation that results in a nonparallel reduction in enzyme activity.

EXPERIMENTAL PROCEDURES

Materials. Chemicals, biochemicals, buffers, and solvents were purchased from Sigma-Aldrich Chemical Co. (St. Louis, MO), Fisher Scientific Inc. (Pittsburgh, PA), Fluka Chemical Corp. (Milwaukee, WI), or EM Science (Cincinnati, OH). The Centricon and Ultrafree centrifugal filter devices were obtained from Millipore Co. (Billerica, MA). Nickel-nitrilotriacetic acid-agarose, a QIAspin kit, and high-throughput crystal condition screens were purchased from QIAGEN. Additive HT Screen was purchased from Hampton Research. The QuikChange site-directed mutagenesis kit was purchased from Stratagene. SAICAR was prepared enzymatically from AICAR purchased from Sigma-Aldrich Chemical Co. as described by Zikanova et al.[24] Enzymes and reagents used for molecular biology procedures were obtained from New England Biolabs, Inc. (Ipswich, MA). The sources for the components of Luria-Bertani (LB) media have been reported previously.[15]

Site-Directed Mutagenesis, Enzyme Expression, and Purification. The initial WT ADSL construct was obtained from R. F. Colman (Department of Chemistry and Biochemistry, University of Delaware, Newark, DE). The full description of the initial WT ADSL construct was published by Lee and Colman.[20] In short, the full-length human ADSL gene (residues 1−484) was constructed in a pET-14b vector containing a 5′-end *Nde*I restriction site and a 3′-end *Blp*I restriction site and a thrombin cleavable N-terminal histidine tag. To overexpress the human enzyme in *E. coli*, the vector was transformed into *E. coli* Rosetta 2(DE3)pLysS. WT and R303C ADSL were purified to homogeneity using a Qiagen Ni-NTA column. Purity was assessed by SDS−PAGE (data not shown). After purification, protein was stored in enzyme storage buffer [50 mM potassium phosphate buffer (pH 7.0) containing 150 mM KCl, 1 mM DTT, 1 mM EDTA, and 10% (v/v) glycerol] at −80 °C. Introduction of point mutations into the human ADSL plasmid was accomplished using QuikChange site-directed mutagenesis. The QIAspin kit was used for cDNA extraction and purification. DNA sequencing was performed at the University of Colorado Cancer Center DNA Sequencing and Analysis Core to confirm mutations. Slight modifications were made to the purification for ITC and X-ray crystallography. Following the purification using the Qiagen Ni-NTA column, thrombin was added to the eluted fraction and it was dialyzed overnight at 4 °C in ADSL running buffer [5 mM HEPES (pH 7.0), 150 mM KCl, and 2 mM DTT] to cleave the His tag. The protein was purified by size exclusion chromatography using S200 Sepharose resin and concentrated to 10 mg/mL for crystallography and to 200−400 μM for ITC. Concentrations were measured by the absorbance at 280 nm using an experimentally determined extinction coefficient of 0.782 L g^{-1} cm^{-1} (43150 M^{-1} cm^{-1}) for thrombin-cleaved ADSL and 0.770 L g^{-1} cm^{-1} for His-tagged ADSL following previously established procedures.[25]

Static Light Scattering. Size exclusion chromatography−multiangle light scattering measurements were performed on a Wyatt miniDAWN TREOS instrument connected to a Shimadzu UFLC and a Wyatt WTC-030S5 size exclusion column. Samples of 350 μg of His-tagged ADSL diluted in enzyme storage buffer were run in duplicate. PBS was used as the mobile phase at a rate of 0.5 mL/min. Calibration was checked using 2 mg/mL bovine serum albumin. Data were analyzed with ASTRA, with a d*n*/d*c* value of 0.185.

Enzyme Assays and Kinetic Studies. Enzyme kinetic experiments were performed on an Evolution 3000 UV−vis spectrophotometer from Thermo Scientific using 1 mL quartz cuvettes at 25 °C. ADSL with the His tag intact was used for enzyme assays, as it has been shown that the His tag does not affect ADSL activity for SAMP.[26] Experiments were conducted with concentrations of 0.11 and 0.19 mg/mL for WT and R303C ADSL, respectively. Frozen samples were incubated for ∼2 h at 25 °C before measurements were taken to ensure the restoration of full activity.[26] SAMP enzyme assays of ADSL were measured in triplicate at 25 °C in 40 mM Tris-HCl (pH 7.4) with varying concentrations of SAMP (1−60 μM). The specific activity was measured from the decrease in absorbance of SAMP at 282 nm as it was converted to AMP and fumarate. The assay was monitored over 30 s in a 1 mL volume. The difference in extinction coefficient of 10000 M^{-1} cm^{-1} between SAMP and AMP was used to calculate the specific activity. SAICAR enzyme assays of ADSL were conducted in triplicate at 25 °C in 40 mM Tris-HCl (pH 7.4) with varying concentrations of SAICAR (1−100 μM). The specific activity was measured from the decrease in absorbance of SAICAR at 269 nm as it was converted to AICAR and fumarate. The assay was monitored over 30 s in a 1 mL volume. The difference in extinction coefficient of 700 M^{-1} cm^{-1} between SAICAR and AICAR was used to calculate the specific activity. To determine the kinetic constants, the initial velocity data were fit to the Hill equation [$v = (V_{max}[S]^n)/(K_{0.5}{}^n + [S]^n)$ for WT and R303C ADSL, and $v = (V_{max}[S])/(K_M + [S])$ for R303C ADSL] using Enzyme Kinetics Module 1.3 of Sigma Plot version 10 (SPSS Inc.). The k_{cat} value was calculated from V_{max} and the enzyme concentration [E] via the equation $k_{cat} = V_{max}/[E]$.

Isothermal Titration Calorimetry (ITC). ITC experiments were conducted using a NANO-ITC system (TA Instruments). Thrombin-cleaved WT ADSL was dialyzed overnight against a solution of 25 mM HEPES (pH 7.0), 150 mM KCl, and 2 mM DTT. AMP was brought to a concentration of 2.5 mM using the buffer in which WT ADSL was dialyzed. ITC runs of WT ADSL with AMP were performed in duplicate and comprised of one injection of 1 μL followed by 24 injections of 2 μL for a total of 25 injections of 2.5 mM AMP into 0.250 mM WT ADSL. Each injection was spaced 250 s apart. ITC experiments were performed in an identical method, injecting AICAR instead of AMP into 0.225 mM WT ADSL. In addition, AMP and AICAR were titrated in an equal manner into 0.280 mM R303C ADSL. Data sets were analyzed with NanoAnalyze and fit to an independent model concurrently with the NanoAnalyze blank constant model to adjust for the heat of dilution. The blank constant model was derived using heats from the last injections deemed by the blank function to be occurring under saturated conditions.

Crystallization of WT and R303C ADSL. Initial crystal conditions for both WT and R303C ADSL were determined from high-throughput screening of Qiagen Nextel screens, Classics and PEG I, in a 96-sitting drop format using an Art Robbins Phoenix robot. The drops consisted of 0.4 μL of protein solution and 0.4 μL of precipitate in a 100 μL reservoir. Initial screening exhibited multiple hits; however, a solution

dx.doi.org/10.1021/bi300796y | *Biochemistry* 2012, 51, 6701−6713

containing 0.1 M Tris (pH 8.0) and 20% (w/v) PEG 6000 produced the most viable crystals for WT ADSL and 0.1 M Tris (pH 8.5) and 20% (w/v) PEG 8000 for R303C ADSL. These crystals were then optimized using Additive HT Screen from Hampton Research. Final WT and R303C ADSL crystals were obtained through vapor diffusion using a 500 μL reservoir with 4 μL drops mixed 1:1 with the protein solution and, for native ADSL, a precipitant gradient of 18 to 28% (w/v) PEG 6000, 0.1 M Tris (pH 8.0), and 12.5 mM $MgCl_2 \cdot 6H_2O$ and, for R303C, a precipitant gradient of 18 to 28% (w/v) PEG 8000, 0.1 M Tris (pH 8.5), and 12.5 mM spermine tetrahydrochloride.

X-ray Structural Determination of ADSL Structures. All X-ray native data sets were collected using crystals mounted on nylon loops and submerged in a 5 μL cryo solution of 26% (w/v) PEG 6000 and 0.1 M Tris (pH 8.0) for WT ADSL and 26% (w/v) PEG 8000 and 0.1 M Tris (pH 8.5) for R303C ADSL. To preserve the crystals, they were submerged and flash-frozen in liquid nitrogen. Frozen crystals were mounted under a stream of dry N_2 at 100 K. A WT ADSL data set with a resolution of 2.70 Å and an R303C ADSL data set with a resolution of 2.60 Å were collected at the 21-ID-D Life Science-Collaborative Access Team beamline at the Advanced Photon Source Synchrotron. Both data sets were collected at 0.9789 Å with a MarMosaic300 CCD detector (Rayonix). All data were subsequently processed and scaled using Scalepack,[27] and subsequent phases were determined and refined using Phaser.[28] Initial models for both WT and R303C ADSL were elucidated by molecular replacement using ADSL structure 2J91 as a search model for Phaser.[28] Both structures were refined using iterative cycles of model building and structure refinement using WinCOOT[29] and REFMAC,[30] respectively. Water molecules were added to $2F_o - F_c$ density peaks that were greater than 1σ using the "Find Water" winCoot program function. The final model was checked for structural quality using the CCP4 suite programs Procheck and Sfcheck. Data processing and refinement statistics are listed in Table 1.

Modeling of AMP/AICAR and Fumarate Binding in the Active Site. Apo structures of WT ADSL with either AICAR or AMP were neutralized with the TLEAP module from the Amber10 simulation package[31,32] and solvated using TIP3P water molecules.[33] The final system was then energy minimized using the Amber 10 simulation package to produce the final structure. Initially, each system's protein was restrained, and the solvent was minimized for 5000 steps to remove any unfavorable contacts that occurred within the water. Then, each system (solvent and molecule) was allowed to energy minimize for 20000 steps, starting with 10000 steps of steepest descent and switching to 10000 more steps of conjugate gradient minimization. The ff99SB force field was used.[34] We removed residues that were more than 30 Å from the AMP/AICAR active site. This was done to reduce computational demand by ignoring distant parts of the protein not relevant for the present problem. However, 30 Å was long enough to focus on a sufficiently large region around the active site to avoid any artifact due to small system size. All the calculations were performed at the University of Denver's High Performance Computing facility, which is a Linux cluster with 22 twin nodes, each node having eight cores.

RESULTS

WT and R303C ADSL Enzyme Kinetics. To ensure that the previously observed reduction in the activity of the ADSL possessing the R303C mutation was not due to aberrant tetramer formation or outright global instability of the mutated protein in solution, static light scattering was employed to determine the polymeric distribution of R303C and WT ADSL. As expected, WT ADSL is predominantly found to be a tetramer, 92.7 ± 2.6%, with aggregates contributing the final percentage. Similarly, R303C ADSL is predominantly a tetramer, 94.3 ± 0.1%, with aggregates contributing the final percentage. Observed masses of the WT and R303C ADSL tetramers were 225.0 ± 2.9 and 214.5 ± 12.2 kDa, respectively, which are in close agreement with the predicted tetrameric masses of the His-tagged WT and R303C ADSL, suggesting that the R303C mutation results in no degradation of the ADSL tetramer.

Previously, a report noted that the ADSL carrying the R303C mutation displayed a nonparallel decrease in activity at a single concentration.[14] Additionally, the kinetic parameters for utilization of SAICAR by human ADSL have never been fully determined. Interestingly, ref 32 details the K_M and k_{cat} of ADSL for SAICAR. Unfortunately, the boundaries of ADSL were not well established at the time of that study, resulting in their use of a 25-amino acid N-truncated version of ADSL and not accounting for cooperativity.[33] Unfortunately, a subsequent study by Kmoch et al.[23] also did not account for ADSL cooperativity, nor did they report on the R303C mutant. This has left ambiguity in the kinetic parameters surrounding the ability of ADSL to use SAICAR as a substrate. To further investigate the R303C phenomenon and determine the K_M and k_{cat} of ADSL for SAICAR, kinetic assays were performed on

Table 1. Data Collection and Refinement Statistics for ADSL

	WT	R303C
Data Collection		
space group	$P2_12_12_1$	$P2_12_12_1$
unit cell dimensions		
a, *b*, *c* (Å)	85.9, 105.2, 215.0	85.8, 105.6, 217.2
$\alpha = \beta = \gamma$ (deg)	90.0, 90.0, 90.0	90.0, 90.0, 90.0
resolution (Å)	50.0−2.70	50.0−2.60
no. of reflections observed	241786	263513
no. of unique reflections	48725	58820
R_{merge} [b] (%)	10.3 (63.1)[a]	12.4 (35.0)[a]
$I/\sigma I$	14.2 (4.3)[a]	18.9 (4.8)[a]
completeness (%)	89.6 (90.2)[a]	95.4 (97.1)[a]
Refinement		
resolution range (Å)	50.0−2.70	50.0−2.60
no. of reflections in the working set	44972	55609
no. of reflections in the test set	2450	2979
R_{work} [c] (%)	24.3	23.0
R_{free} [c] (%)	29.2	29.8
mean *B* factor (Å^2)	27.5	55.1
protein *B* factor (Å^2)	27.6	54.9
water *B* factor (Å^2)	19.2	50.1
rmsd		
bond lengths (Å)	0.01	0.01
bond angles (deg)	0.90	1.01
no. of atoms (protein/water)	14605/214	14764/144
no. of monomers in the asymmetric unit	4	4

[a]Data for the last resolution shell are given in parentheses. [b]$R_{merge} = \sum_h \sum_i |I_i(h) - \langle I(h)\rangle| / \sum_h \sum_i I_i(h)$, where $I_i(h)$ is the *i*th measurement and $\langle I(h)\rangle$ is the weighted mean of all measurements of $I(h)$. [c]R_{work} and $R_{free} = h[|F(h)_o| - |F(h)_c|]/h|F(h)_o|$ for reflections in the working and test sets, respectively.

dx.doi.org/10.1021/bi300796y | Biochemistry 2012, 51, 6701−6713

both WT and R303C ADSL using SAICAR and SAMP as substrates.[14] Both WT and R303C ADSL had measurable activity that could be evaluated by monitoring the UV absorbance of either SAMP or SAICAR. As WT ADSL was previously reported not to follow simple Michaelis–Menten kinetics for SAMP and perhaps be cooperative, the Hill equation was initially employed for calculating WT ADSL's kinetic parameters (Table 2 and Figure S1 of the Supporting Information).[20] The resulting Hill coefficients of WT ADSL for SAMP and SAICAR are both significantly above 1, indicating cooperativity for the substrates. The resulting k_{cat} and $K_{0.5}$ of WT ADSL for SAMP were in agreement with a prior study that utilized the nontruncated form of ADSL.[20] For WT ADSL's utilization of SAICAR, its $K_{0.5}$ was 1.8 ± 0.1 μM, which is only slightly higher than SAMP's. However, WT ADSL's k_{cat} for SAICAR was 1.6-fold higher than that for SAMP, suggesting that ADSL is more kinetically efficient for the catalysis of SAICAR over SAMP. This is confirmed by WT ADSL's $k_{cat}/K_{0.5}$ for SAICAR being 2-fold higher than SAMP's. Additionally, the k_{cat} for both substrates was found not to be diffusion-limited.

Table 2. Enzymatic Activities of ADSL with SAMP and SAICAR at 25 °C[a]

	SAMP		SAICAR	
	WT	R303C	WT	R303C
$k_{cat,H}$ (s^{-1})	52.2 ± 1.8	2.33 ± 0.07	90.2 ± 1.9	27.8 ± 0.8
$k_{cat,H}$ (%)	100 ± 3	4.5 ± 0.1	100 ± 2	31 ± 1
$K_{0.5}$ (μM)	2.1 ± 0.2	2.3 ± 0.12	1.8 ± 0.1	8.4 ± 0.8
Hill coefficient	1.5 ± 0.2	1.03 ± 0.08	1.22 ± 0.09	0.94 ± 0.06
$k_{cat,H}/K_{0.5}$ (s^{-1} μM^{-1})	25.0	0.99	49.6	3.37
$k_{cat,M}$ (s^{-1})	N/A[b]	2.36 ± 0.04	N/A[b]	27.2 ± 0.4
$k_{cat,M}$ (%)	N/A[b]	4.5 ± 0.1	N/A[b]	30 ± 1
K_M (μM)	N/A[b]	2.4 ± 0.2	N/A[b]	7.8 ± 0.4
$k_{cat,M}/K_M$ (s^{-1} μM^{-1})	N/A[b]	0.99	N/A[b]	3.45

[a] k_{cat}, $K_{0.5}$, K_M, and the Hill coefficient were determined by varying substrate concentration and fitting data to the Hill equation (H) or the Michaelis–Menten equation (M) in Sigma Plot. Protein was reconstituted for 2 h at 25 °C prior to measurements. R303C activity is relative to the WT percentage. The values are shown along with their standard errors. [b] Not applicable.

Introduction of the R303C mutation into ADSL has multiple effects. Initially expecting a cooperativity similar to that observed in WT ADSL, we utilized the Hill equation (Table 2). Unlike WT ADSL, R303C ADSL demonstrates no cooperativity, with a Hill coefficient for both substrates of 1. As a result, the simple Michaelis–Menten equation was employed for R303C. The R303C ADSL mutation reduces k_{cat} to 4.5 and 30% of that relative to WT ADSL for SAMP and SAICAR, respectively. Interestingly, this 7-fold difference in residual in vitro activity is in line with cell free extract studies of a type II patient's fibroblasts carrying the R303C mutation, which had 3% of normal SAMP activity and 30% of normal SAICAR activity.[22,35] As a result, the SAICAR:SAMP ratio of activity of WT ADSL is 1.7, which is in agreement with a previously published ratio of 1.6, but the ratio of activity for R303C ADSL shifts to 11.5.[21] Interestingly, K_M values of R303C ADSL increased for SAICAR compared to that of WT ADSL. The change observed in the K_M of R303C ADSL for SAMP is almost negligible, with the K_M for SAICAR increasing more than 4-fold. This may initially suggest the mutation affects the ability of R303C ADSL to bind SAICAR more than SAMP, resulting in the disparity in their cleavage. However, the rate of SAICAR cleavage by R303C ADSL is 5 times more rapid than that for SAMP at R303C ADSL's SAMP K_M. Therefore, the effect of the R303C mutation on ADSL may not solely be reflective of its divergent ability to bind SAICAR and SAMP. It suggests that R303C may affect the catalytic mechanism of SAMP and SAICAR in addition to binding of the substrates.

Isothermal Titration Calorimetry (ITC). To explore the possible thermodynamic factors involved in the nonparallel reduction in activity resulting from the R303C mutation and in general ADSL–substrate interactions, we performed ITC on WT and R303C ADSL with their products AMP and AICAR. By measuring the amount of heat liberated per injection as a function of the molar ratio of the substrate and protein, we calculated thermodynamic parameters for R303C and WT ADSL's interaction with their products (Table 3 and Figure S2 of the Supporting Information). Intriguingly, product binding does not show any evidence of cooperativity, as the data fit to an independent model rather than a multiple-binding site model. This does not necessarily rule out the possibility that substrate binding is cooperative but suggests that cooperativity may require inclusion of interactions between the fumarate component of the substrates and ADSL, which is lacking in the products.

Beyond the observed absence of cooperativity, the K_d values for WT ADSL were 54 and 34 μM for AMP and AICAR, respectively (Table 3 and Figure S2a,b of the Supporting Information). The thermodynamic properties that are responsible for binding of AICAR and AMP to WT ADSL globally are similar, with the enthalpic component, ΔH, being the predominant driving force and the entropic component, ΔS, being unfavorable. Although similar, the thermodynamic

Table 3. ITC Thermodynamic Parameters of ADSL[a]

	AMP		AICAR	
	WT	R303C	WT	R303C
K_d (μM)	54 ± 3	130 ± 8	34 ± 2	121.9 ± 0.9
ΔH (kJ mol^{-1})	−35 ± 2	−5.9 ± 0.2	−53 ± 1	−16.7 ± 0.5
$T\Delta S$ (kJ mol^{-1})	−12 ± 1	15.92 ± 0.06	−28 ± 1	5.3 ± 0.5
ΔG (kJ mol^{-1})	−23.9 ± 0.1	−21.8 ± 0.2	−25.1 ± 0.1	−21.95 ± 0.02
n	0.99 ± 0.01	1.01 ± 0.04	1.00 ± 0.02	1.00 ± 0.02

[a] Data sets were collected in duplicate and analyzed with NanoAnalyze and fit to an independent model concurrently with a blank constant model to adjust for the heat of dilution. All measurements were from 25 injections of 2.5 mM AMP into 170 μL of protein in 25 mM HEPES (pH 7.0), 150 mM KCl, and 2 mM DTT at 20 °C.

dx.doi.org/10.1021/bi300796y | Biochemistry 2012, 51, 6701–6713

properties are not identical. AICAR binding liberates an additional 18 kJ/mol, suggesting an additional hydrogen bond may be formed between AICAR and WT ADSL that is absent in a AMP and WT ADSL complex. The lack of this additional enthalpic contribution is partially offset in the AMP and WT ADSL complex by the reduced unfavorable entropic component compared to that of the AICAR and WT ADSL complex. Overall, this leads to a difference in ΔG between binding of AMP and AICAR to WT ADSL of only 1.2 kJ/mol in AICAR's favor.

Intriguingly, the R303C mutation impacts the ability of ADSL to form a complex with AMP and AICAR in two distinct manners. The enthalpic component for both products decreases by a similar degree of ~30 kJ/mol, suggesting the loss of one to two hydrogen bonds, whose identity could be common between the two products and ADSL. Additionally, the R303C mutation shifts the formation of the ADSL complex with AMP and AICAR from an unfavorable to favorable entropic event. Taken together, these thermodynamic factors result in a similar decrease in ΔG and increases of 76 and 88 μM in the K_d values of AMP and AICAR, respectively. As a result, the R303C mutation appears to negatively affect ADSL's interaction with AMP and AICAR almost indistinguishably.

X-ray Structural Elucidation of R303C and WT ADSL. Recently, a study proposed that the R303C mutation may distort the active site cleft.[14] To investigate the structural effects of the R303C mutation on ADSL and how these effects might be linked to the lower activity and unique specificity of ADSL with the R303C mutation, the crystal structure of R303C ADSL (R303C-ADSL) was elucidated to 2.60 Å. A homotetramer in the asymmetrical unit was observed, with each monomer composed of 16 α-helices and three small β-sheets, which can be further divided into three domains (Figures 1 and 2). Electron density was observed for the majority of ADSL residues 5−476 in all monomers, with residues 5−112 forming domain 1, residues 113−364 forming domain 2, and residues 364−476 forming domain 3. A notable exception was the range of residues 286−291 in all monomers. These residues comprise the β3−α10 loop (also known as the C3 loop), which is located near ADSL's active site and expected to contain an important catalytic serine, S289. The lack of density for this region is not fully unexpected, as it has been unobserved in all but one bacterial ADSL X-ray structure. As a result, the loop is suggested to be highly flexible (Figure 1). Apart from the expected differences in the positions of the residues just prior to and after the missing density of the β3−α10 loop, the only other notable difference observed among the four monomers of R303C-ADSL resides in domain 3 of the structure. This domain is on the periphery of the tetrameric complex, likely resulting in the small alterations and higher *B* factors among the four monomers in that region (Figure 2).

Despite these differences on the periphery of the protein, from a distance R303C-ADSL globally resembles PDB entry 2VD6 with its four active sites a mixture of active site-bound SAMP, or AMP with fumarate (ADSL-SAMP) as well as AMP-bound ADSL (PDB entry 2J91) (ADSL-AMP). Unlike ADSL-AMP in which all of the active sites are indistinguishably bound to AMP, ADSL-SAMP has its active sites 1 and 2 filled with AMP and fumarate, while SAMP was observed in active sites 2 and 4 (Figure 3a,b). Both of these ligand-bound structures previously have alluded to ADSL active sites being formed by three contributing monomers. For example, in active site 1, the monophosphate group of AMP hydrogen bonds to three

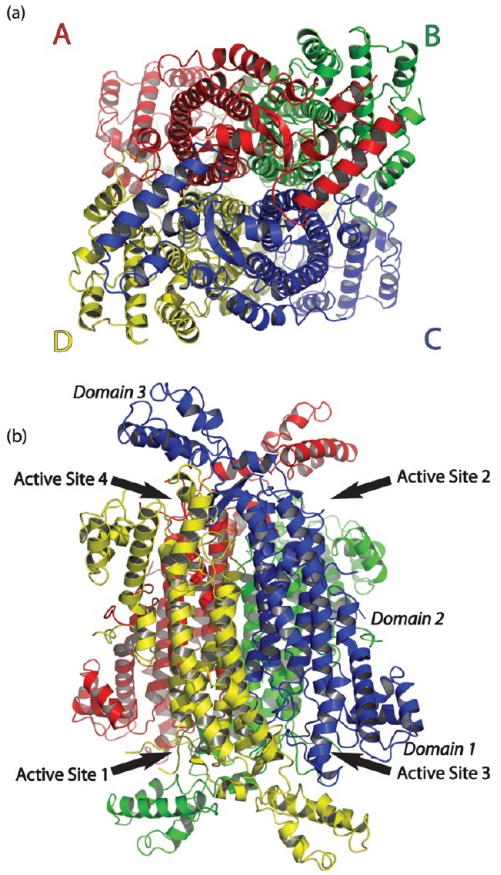

Figure 2. Side and top views of the WT homotetramer. $P2_12_12_1$ asymmetric unit of the WT crystal. Monomers A−D are colored red, green, blue, and yellow, respectively. Domains 1−3 are indicated for monomer C. Active sites are denoted with arrows.

residues from chain A. The fumarate interacts with three residues from chain A bridging across to interactions with two residues from chain B and one from chain D (Figure 3a). The ADSL-SAMP active sites with SAMP bound have similar intermonomeric interactions (Figure 3b). Not surprisingly, upon inspection of the corresponding active site of R303C ADSL, density for the R303 side chain is largely absent, with only enough remaining to represent a mutation to cysteine at that position (Figure 3c and Figure S3 of the Supporting Information). On the basis of the ligand-bound structures, this mutation would appear to simply eliminate the hydrogen bonds formed between the monophosphate in the AMP, or SAMP, and ADSL. This loss of the phosphate−R303 interaction, which also likely exists with AICAR, could be reflected in the enthalpy change detected by ITC for AMP and AICAR. However, upon closer examination, superimposition of the active sites of R303C-ADSL with the corresponding sites in ADSL-SAMP revealed that the two structures' corresponding active sites are not entirely identical, giving possible credence to an earlier study's suggestion that the R303C mutation may disrupt the active site cleft.[14] Specifically, comparison of R303C-ADSL's active sites with ADSL-SAMP's corresponding fumarate and AMP-bound active sites shows a 2.5 Å shift of α-helices 2−4 (Figure 4a). This shift is also observed between R303C-ADSL and ADSL-AMP. Interestingly, similar, but not exact, shifts are also observed between R303C-ADSL's active sites and the SAMP-filled active sites of ADSL-SAMP. To determine if the shift in α-helices 2−4 was related to the R303C mutation or a

dx.doi.org/10.1021/bi300796y | *Biochemistry* 2012, 51, 6701−6713

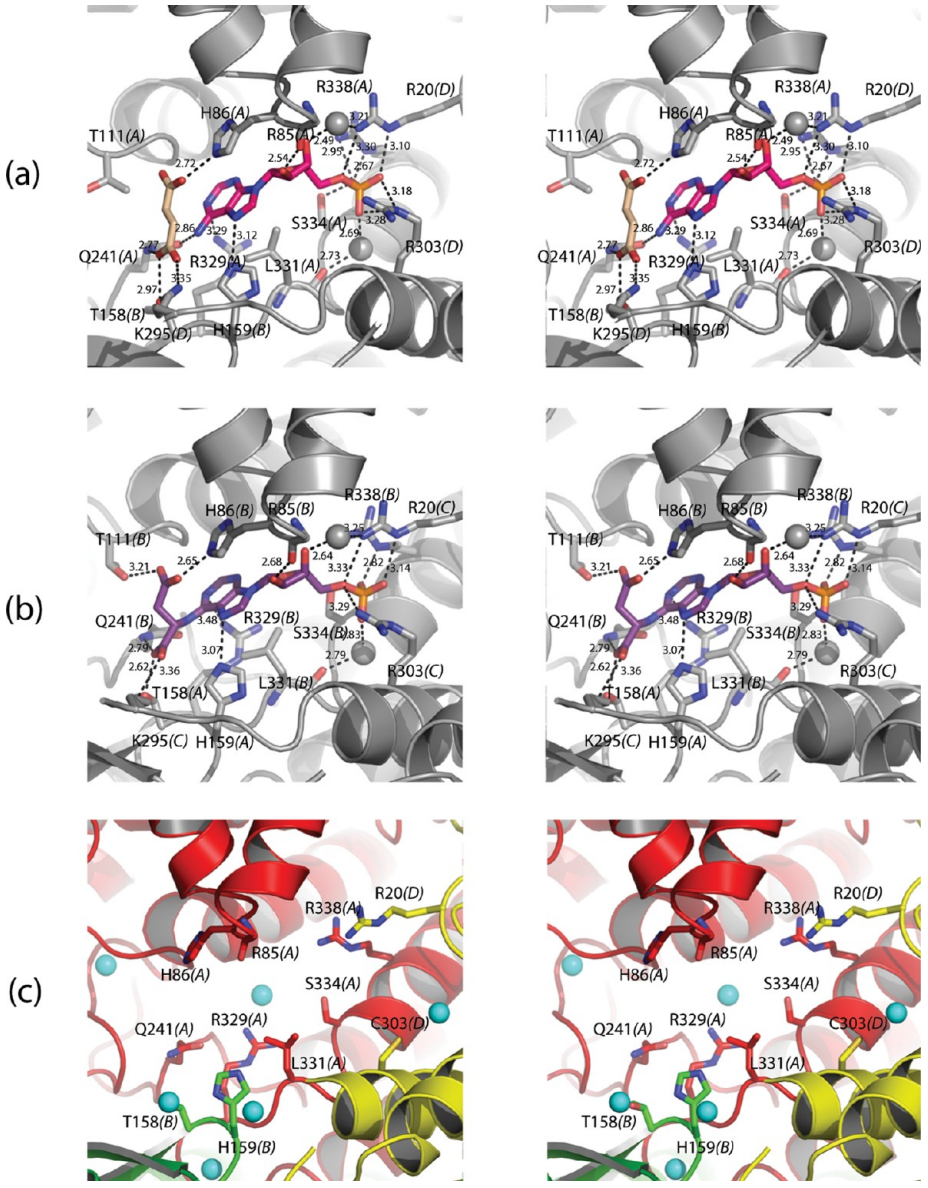

Figure 3. Comparison of ADSL active sites for WT, WT with a substrate, and the R303C mutant. (a) Wall-eyed stereoview of an ADSL-SAMP active site with AMP and fumarate occupying the active site. AMP is colored pink and fumarate tan. Heteroatoms are colored according to their element. Water molecules (gray) are depicted as spheres and are scaled to 50% for the sake of clarity. The monomer to which each residue belongs is given in parentheses after the residue number. (b) Wall-eyed stereoview of an ADSL-SAMP active site with SAMP occupying the active site. SAMP is colored purple, and heteroatoms are colored according to their element. Water molecules (gray) are depicted as spheres and are scaled to 50% for the sake of clarity. The monomer to which each residue belongs is given in parentheses after the residue number. (c) Wall-eyed stereoview of the R303C ADSL active site. Monomers A, B, and D are colored red, green, and yellow, respectively. Heteroatoms are colored according to their element. Water molecules (cyan) are depicted as spheres and are scaled to 50%, and the side chain of R85 is hidden for the sake of clarity. The monomer to which each residue belongs is given in parentheses after the residue number.

conformational change related to substrate binding, the structure of WT ADSL in its apo form (WT ADSL-apo) was elucidated to 2.70 Å (Figure 4b). As for R303C-ADSL and ADSL-SAMP, electron density for residues 283−293 (β3−α10 loop) was not observed. Like R303C-ADSL, WT ADSL's monomers were largely indistinguishable outside of domain 3. Intriguingly, comparison of WT ADSL-apo with ADSL-SAMP revealed a 2.7 Å shift of α-helices 2−4 in line with those observed previously in the comparison of R303C-ADSL versus ADSL-SAMP, indicating that substrate binding is likely the major cause of the shifts observed between R303C-ADSL and ADSL-SAMP (Figure 4c), while comparison of WT ADSL-apo to R303C-ADSL revealed nearly identical structures (Figure 4d). In addition, WT ADSL-apo reveals an additional apo form of the ADSL active site that is divergent from product- and substrate-bound active sites previously observed.

Modeling of AMP/AICAR and Fumarate Binding in the Active Site. Currently, no crystal structure for WT ADSL with AICAR bound has been determined. Utilizing the elucidated WT ADSL-apo and ADSL-SAMP structures along with an understanding of local active site shifts within the active site upon substrate binding, AICAR and fumarate were modeled into the active site. Specifically, the AMP- and fumarate-bound active site of PDB entry 2VD6 was employed as a template for the initial location of AICAR and fumarate within an active site of WT ADSL-apo. Using the Amber10 simulation package, by

dx.doi.org/10.1021/bi300796y | *Biochemistry* 2012, 51, 6701−6713

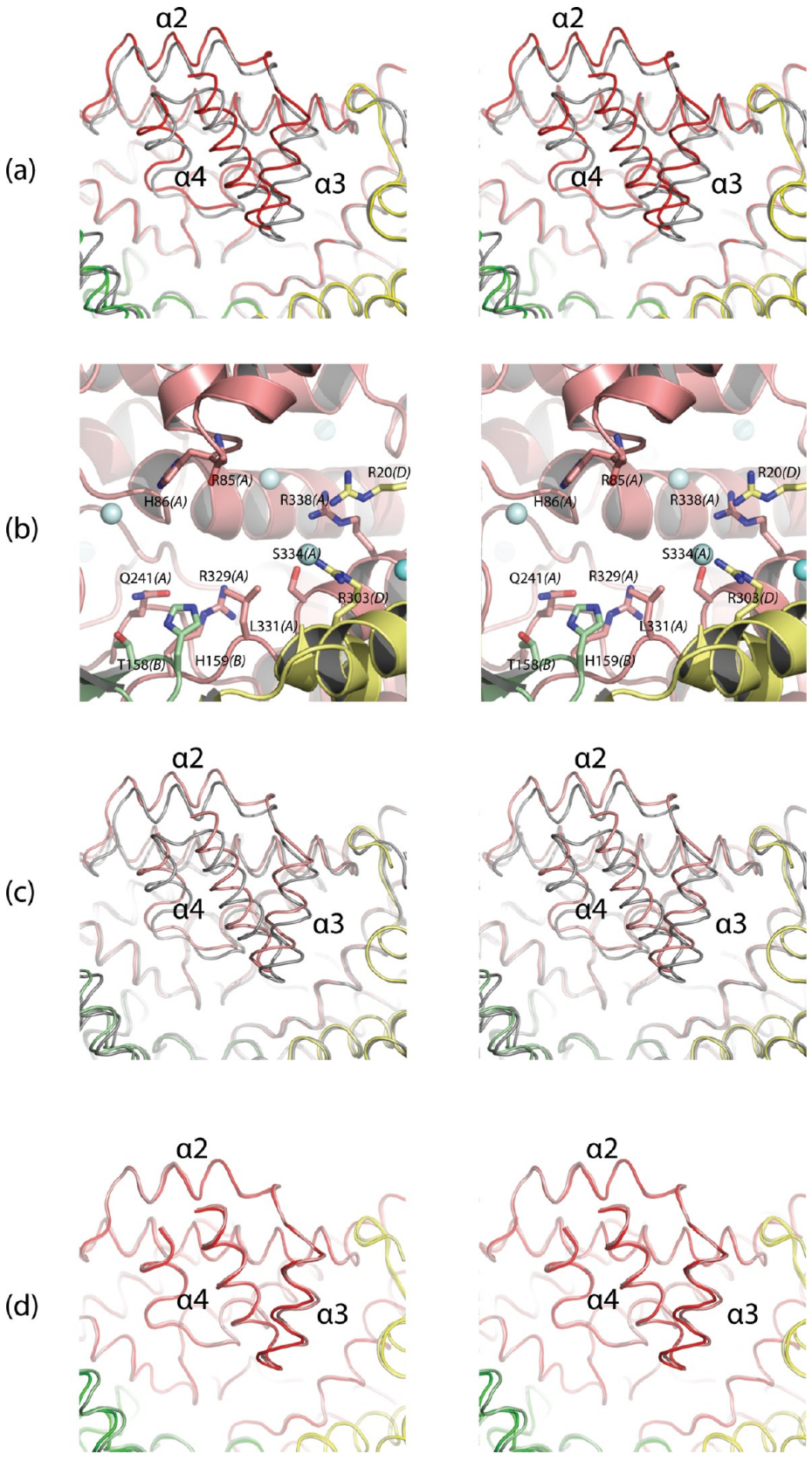

Figure 4. Substrate-induced shifts of α-helices 2−4. (a) Wall-eyed stereoview comparing the mobile α2−α4 loop between ADSL-SAMP (gray) and R303C-ADSL. (b) Wall-eyed stereoview of the WT active site colored salmon, light yellow, and pale green, with waters colored aqua. Heteroatoms are colored according to their element. Water molecules are depicted as spheres and are scaled to 50%, and the side chain of R85 is hidden for the sake of clarity. The monomer to which each residue belongs is given in parentheses after the residue number. (c) Wall-eyed stereoview comparing the mobile α2−α4 loop between ADSL-SAMP and WT ADSL-apo. Coloring is as in panels a and b. (d) Wall-eyed stereoview comparing the mobile α2−α4 loop between R303C-ADSL and WT ADSL-apo. Coloring is as in panels a and c.

dx.doi.org/10.1021/bi300796y | *Biochemistry* 2012, 51, 6701−6713

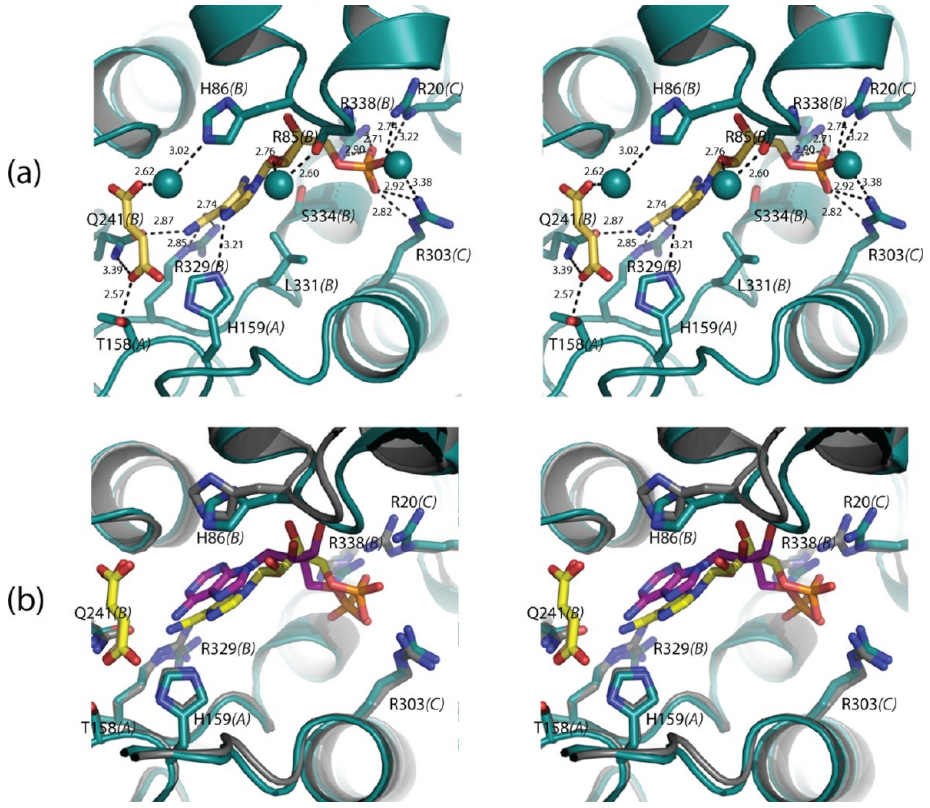

Figure 5. ADSL-AICAR-fumarate model. (a) Wall-eyed stereoview of the model of the WT active site with AICAR and fumarate occupying the active site. AICAR and fumarate are colored yellow. Heteroatoms are colored according to their element. The monomer to which each residue belongs is given in parentheses after the residue number. (b) View of the model of the WT active site with AMP and fumarate overlaying the model of WT active site with AICAR and fumarate. WT with AMP is colored gray with AMP in pink and fumarate colored tan, while WT with AICAR residues are colored teal with AICAR and fumarate colored yellow.

energy minimization the ADSL-AICAR-fumarate model structure was determined (Figure 5a). To validate the modeling parameters that were used, we also energy minimized the structure with AMP and fumarate instead in the WT ADSL-apo active site. The resulting AMP- and fumarate-bound ADSL model was nearly identical to that of AMP- and fumarate-bound ADSL-SAMP.

As is evident from the figure, the placement of the fumarate, phosphate, and ribose groups of AICAR and SAMP within the ADSL active site is similar (Figure 5b). However, the remaining structure of the two substrates forms divergent interactions within the active site. This divergence could be a result of a rotatable bond between AICAR's imidazole ring and carbonyl carbon, whereas the presence of the pyrimidine in AMP eliminates the ability of the corresponding bond to rotate.[36] As a result, this flexibility in AICAR and an amine group substituent of its imidazole ring potentially allow the amine to stick out in a space previously occupied by a water molecule potentially facilitating a hydrogen bond with the hydroxyl group of the conserved S334 (Figure 1). Additionally, the rotation of the AICAR amide causes an alteration in the R329 side chain to form a hydrogen bond with AICAR's amide group.

DISCUSSION

Origins of ADSL Cooperativitiy. The elucidation of the ADSL-SAMP structure has previously been suggested to support cooperativity in human ADSL, as AMP and fumarate are found in two active sites and with the other two occupied by SAMP. However, previously limited biochemical data supported the origins or form of cooperativity found in ADSL. Interestingly, the kinetic and thermodynamic properties of WT ADSL and the R303C mutant suggest that the involvement of all three monomers that comprise an ADSL active site is necessary to achieve ADSL's positive cooperativity. Specifically, no cooperativity was observed when AICAR, or AMP, binds to WT ADSL. Binding of these products forms the majority of their interactions with only two of the monomers. For example, in active site 1, AMP interacts with six residues from monomer A and one from monomer B. Additionally, the phosphate group of AMP is anchored with two additional residues from a relatively immobile portion of monomer D (Figure 3a). This leaves the fumarate product to span interactions among monomer A's mobile α-helices 2−4, monomer B, and the near β3−α10 catalytic loop region of monomer D, suggesting that it is necessary for cooperativity to be observed. In line with this hypothesis, mutation of R303 to cysteine, which removes two hydrogen bonds, thus removing the majority of the interactions between monomer D and SAMP, results in no cooperativity (Figure 3b).

Beyond the necessity for the substrate, or products, to involve all three monomers when binding to achieve an allosteric response, comparison of the WT ADSL-apo and ADSL-SAMP active sites provided a glimpse into the model of allosteric regulation that ADSL employs. Specifically, the WT ADSL-apo active sites are considerably more open to the bulk solvent then those of the ADSL-SAMP and ADSL-AMP structures (Figure 6a). The 2.7 Å shift of α-helices 2−4

dx.doi.org/10.1021/bi300796y | *Biochemistry* 2012, 51, 6701−6713

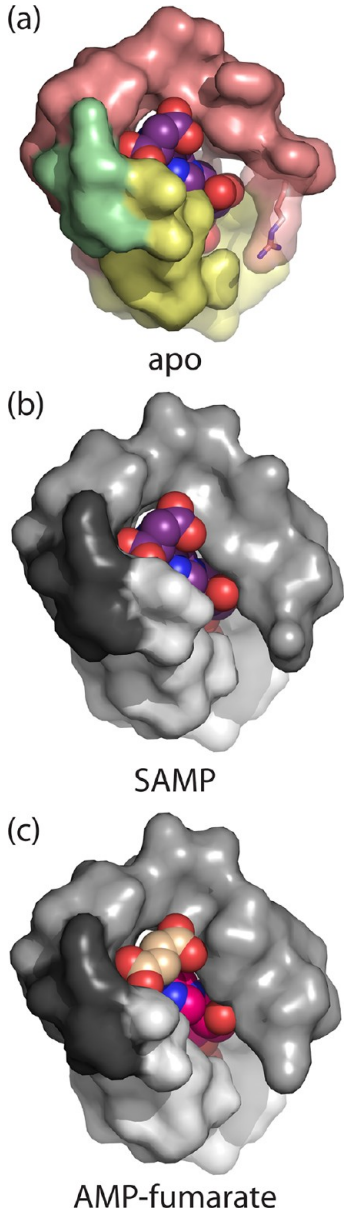

Figure 6. Constriction of the ADSL active site upon substrate binding. (a) Surface rendering of WT ADSL-apo active site 1. The WT active site is colored salmon, light yellow, and pale green, corresponding to monomers A, B, and D, respectively. The R85 side chain is shown with transparency to reflect the lack of electron density for the side chain in all monomers. AMP and fumarate from active site 1 of ADSL-SAMP were placed in the apo active site for scaling purposes. (b) Surface rendering of SAMP- and fumarate-bound active site 1 of ADSL-SAMP. Light gray, medium gray, and dark gray correspond to monomers A, B, and D, respectively. (c) Surface rendering of the SAMP- and fumarate-bound active site of ADSL-SAMP. Light gray, medium gray, and dark gray correspond to monomers A, D, and C, respectively. All waters were removed from surface renderings in panels a–c.

observed between the WT ADSL-apo active sites and those bound with AMP, or AMP and fumarate, illustrates a clamping down of the active site over SAMP, or AMP. With AICAR and SAICAR having phosphate, fumarate, and ribose moieties homologous to that of AMP, the same shift is likely to occur upon the binding of these ligands as well. This closure of the active site around SAMP suggests that a concerted model of allosteric regulation would not be possible (Figure 6c). In other words, if this shift occurred in a neighboring active site as a result of binding of SAMP and SAICAR for the reaction running in the forward direction, SAMP attempting to bind to the neighboring active site would be sterically impeded. This would not be reflective of the positive cooperativity observed. Applying sequential allosteric regulation to the reverse reaction is less certain. The binding of AMP and AICAR would also be sterically impeded from binding to an active site that already underwent a shift of α-helices 2–4. However, as illustrated by the thermodynamic information, the binding of AMP and AICAR does not illustrate cooperativity. With fumarate binding at the top of the active site, which is exposed to the bulk solvent, a concerted model in the reverse direction cannot be ruled out (Figure 6b).

Beyond the sequential model of allosteric modulation of ADSL, the order in which or the extent to which the active sites fill with substrates remains an open question. The ADSL-SAMP structure has its two active sites on the same end of ADSL occupied by SAMP and other distal active sites bound with fumarate and AMP. The absence of SAMP in all of the active sites could be due to restraints of the enzyme imposed by the crystal lattice but alternatively might propose that substrates bind to adjacent active sites first or can bind to only them. The latter would infer that the active sites at one end of the ADSL tetramer communicate to its distal neighbors. Although the mild loss of cooperativity observed by Ariyananda et al.[20] by an ADSL L311V mutation at the center of the tetramer would support this possibility, additional structurally guided mutagenesis along the monomer's interface and molecular dynamics simulations will be required to completely tease out the global allosteric nature of ADSL.

Catalytic Effects of the R303C Mutation. The loss of cooperativity because of the removal of hydrogen bonds by the R303C mutation with one of the three monomers comprising the active site as reflected in the structures of ADSL-SAMP, or ADSL-AMP, would not itself explain the divergent catalytic properties of ADSL observed toward SAICAR and SAMP. However, the combination of the kinetic and thermodynamic data coupled with the structural evidence suggests that the R303C mutation illuminates SAICAR as a better substrate for ADSL. At first glance, the unparallel reduction in k_{cat} between SAMP and SAICAR upon the R303C mutation could suggest that the divergence in the catalytic ability of ADSL between SAMP and SAICAR is due to a lack of substrate binding that favors SAICAR, or AICAR binding over that of SAMP. However, the K_M for SAICAR is slightly elevated relative to that of SAMP, indicating that binding of SAICAR might be slightly weaker (Table 2). Moreover, the ADSL ligand-bound structures have R303 forming hydrogen bonds to the phosphate group that is conserved between SAICAR and AICAR (Figure 3). Also, the thermodynamic data reflect the fact that the mutation causes losses of enthalpy almost equal in magnitude for both AICAR and AMP, reflective of a loss of the same ADSL–phosphate group interactions. Despite the loss of the bond to the phosphate group, the overall ΔG_{bind} for both products remains similar to that of WT ADSL. This is accomplished by shifting the product binding from an unfavorable to a favorable entropic event. The resulting K_d values for both substrates are nearly equally decreased by approximately 2.5–3-fold. This near equal drop in K_d but not k_{cat} suggests that the R303C mutation is indirectly affecting the catalytic ability of ADSL divergently for its two substrates. In other words, this thermodynamic, kinetic, and structural

dx.doi.org/10.1021/bi300796y | *Biochemistry* 2012, 51, 6701–6713

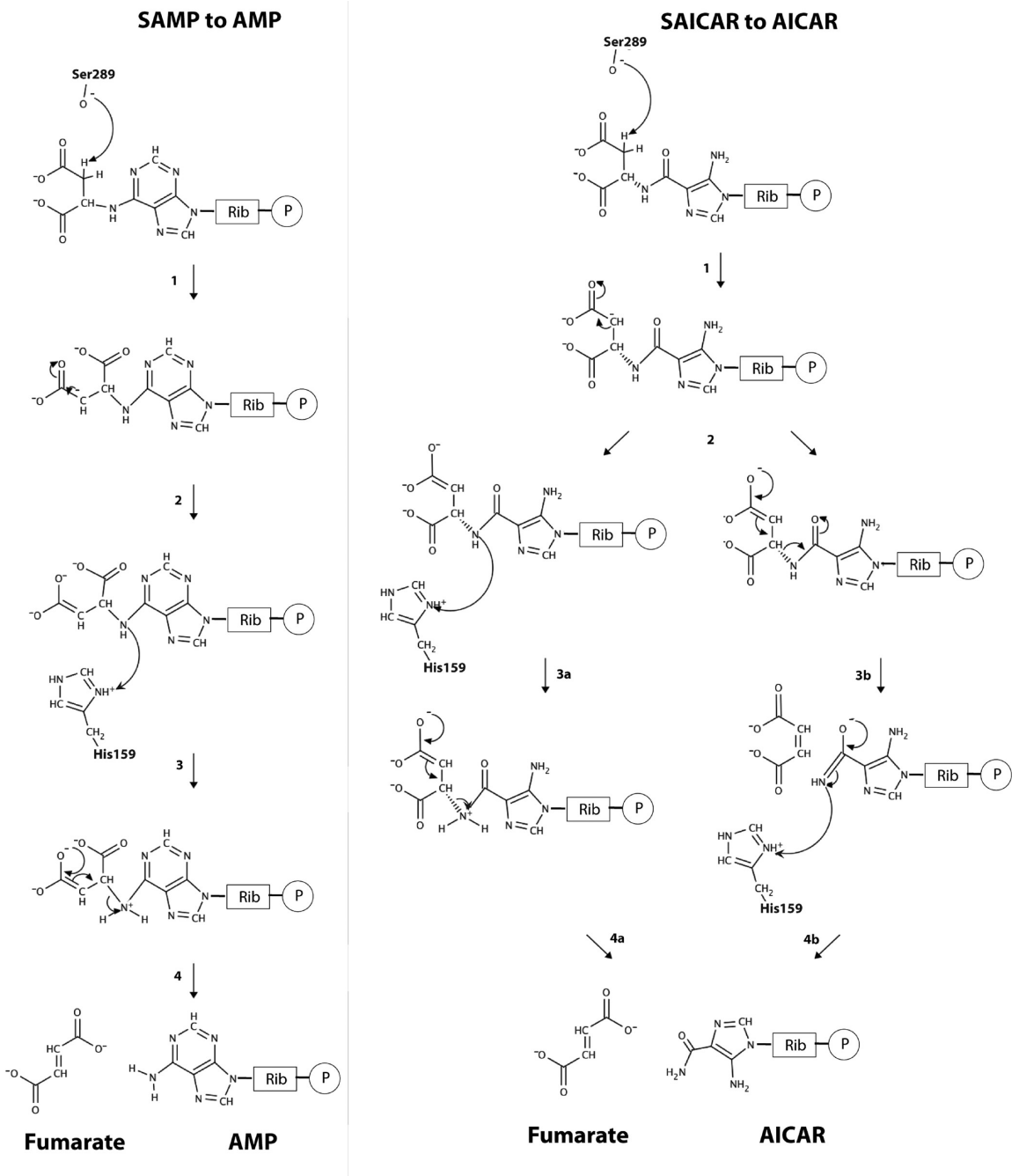

Figure 7. Proposed mechanism for SAICAR to AICAR and fumarate and for SAMP to AMP and fumarate.

evidence suggests that the substrate can bind to the active site with a significant affinity despite the R303C mutation. As a result, unlike WT ADSL, the R303C mutant is likely operating in a rapid equilibrium state, where if the substrate binds to ADSL, most substrate will dissociate, and only a small amount will be converted to product.

This would suggest that ADSL is more efficient at cleaving the fumarate−AICAR/AMP bond of SAICAR than that of SAMP. The inequality of catalysis might suggest that SAICAR and SAMP do not follow the same mechanistic pathway. The reaction mechanism for conversion of SAMP and SAICAR by ADSL has been previously described as a general acid−base mechanism resulting in β-elimination of fumarate (Figure 7).[16] Although the conversion of SAICAR to AICAR and fumarate could follow the same steps as the SAMP to AMP mechanism, because of the presence of an additional carbonyl in SAICAR, there is another possibility. In this SAICAR selective pathway, the first two steps are the same: the C^{β} proton is removed, and the negative charge is stabilized by the δ-carboxyl group. However, in the third step, as the electron density from the doubly negatively charged carboxyl group is shifted down and the C^{α}−N6 bond is broken, a double bond is formed between N6 and the carbonyl carbon, and electron density is pushed up onto the carbonyl oxygen. Then, in the last step, this negative charge moves back down to form a C−O double bond as N6 becomes protonated by H159. This negatively charged oxygen may be stabilized by nearby positively charged residue R235. This additional stabilization of the intermediate may be a factor

dx.doi.org/10.1021/bi300796y | *Biochemistry* 2012, 51, 6701−6713

in the faster reaction rate of SAICAR compared to that of SAMP.

An alternative possibility, or a potential additional factor, for the inequality of bond cleavage between SAMP and SAICAR is the ability of SAICAR to be positioned with the active site in a more catalytically effective orientation than SAMP. The loss of the hydrogen bonds that R303 contributed to substrate binding potentially affected the ability to orient SAMP and SAICAR ideally for cleavage. Unlike SAMP, which possesses a pyrimidine ring, SAICAR has a single rotatable bond that has been previously suggested to infer greater flexibility to adopt different conformations.[36] This also might explain the lack of unparallel reduction in the catalytic ability of *B. subtilis* ADSL. In that case, *B. subtilis* ADSL has an arginine in place of human ADSL T354 that may have a similar influence. Unfortunately in the study by Palenchar et al. that looked at the *B. subtilis* ADSL corresponding human ADSL R303C mutation (*B. subtilis* ADSL N276C), only a double mutation was performed to mimic the human active site configuration and did not include a mutation for the corresponding arginine at human ADSL's T354. This prevented the observation of whether elimination of anchoring ADSL's substrates by a third arginine resulted in unparallel catalytic ability.

Additionally, the thermodynamic data suggest that AICAR forms an additional hydrogen bond not present in the ADSL-AMP complex. The enthalpic divergence between the two substrates remains after the introduction of the R303C mutation. The ability of SAICAR to possess an additional point of contact within the ADSL active site could ensure that SAICAR is properly oriented within the active site more often than SAMP, contributing to the unparallel k_{cat} between SAMP and SAICAR observed. On the basis of the ADSL-AICAR-fumarate model, the additional hydrogen bond could be reflective of an interaction between AICAR and the highly conserved S334 (Figure 5a). Curiously, even in human ADSL's distant homologue of *B. subtilis*, this serine is conserved. This serine has not previously been implicated in substrate binding or catalysis, as it does not interact directly with SAMP or AMP within the ADSL-SAMP and ADSL-AMP structures. Naturally, additional site-directed mutagenesis efforts within the active site, including S334, or an X-ray structure of ADSL with SAICAR, or AICAR, will be necessary to fully identify the ADSL residue acceptor that forms the additional hydrogen bond with AICAR and bring final clarity to the unparallel catalytic activity observed.

■ ASSOCIATED CONTENT

Supporting Information

Specific activity versus substrate concentration plots of WT and R303C ADSL (Figure S1), calorimetric titration of ADSL with AMP and AICAR (Figure S2), and missing electron density for R303 when it is mutated to cysteine in ADSL (Figure S3). This material is available free of charge via the Internet at http://pubs.acs.org.

Accession Codes

The atomic coordinates and structure factors have been deposited with the Protein Data Bank (entries 4FLC and 4FFX).

■ AUTHOR INFORMATION

Corresponding Author

*Department of Chemistry and Biochemistry (S.D.P.), Department of Biological Sciences (D.P.), and Eleanor Roosevelt Institute (S.D.P. and D.P.), University of Denver, 2101 E. Wesley Ave., Denver, CO 80208. D.P.: telephone, (303) 871-5650; fax, (303) 871-3223; e-mail, david.patterson@nsm.du.edu. S.D.P.: telephone, (303) 871-2533; fax, (303) 871-2254; e-mail, scott.pegan@du.edu.

Author Contributions

S.P.R. and M.K.D. contributed equally to this work.

Funding

This research was supported by the University of Denver's Interdisciplinary Grant Program (K.G., D.P., and S.D.P.) and in part by the University of Denver's Partners in Scholarship (L.A.F.C.) and the Bonfils-Stanton Foundation (D.P.). Data sets were collected at the Life Sciences Collaborative Access Team (LS-CAT) 21-ID-D beamline at the Advanced Photon Source (Argonne National Laboratory, Argonne, IL). Use of the Advanced Photon Source was supported by the U.S. Department of Energy, Office of Science, Office of Basic Energy Sciences, under Contract DE-AC02-06CH11357. Use of the LS-CAT Sector 21 was supported by the Michigan Economic Development Corp. and the Michigan Technology Tri-Corridor for the support of this research program (Grant 085P1000817). The DNA samples were sequenced by the University of Colorado Cancer Center DNA Sequencing and Analysis Core (http://DNASequencingCore.ucdenver.edu), which is supported by a National Institutes of Health/National Cancer Institute Cancer Center Core Support Grant (P30 CA046934).

Notes

The authors declare no competing financial interest.

■ ACKNOWLEDGMENTS

We thank Dr. Roberta F. Colman for her generous gift of the initial ADSL construct. Also, we appreciate Terry G. Wilkinson, II, for the technical support in generating the R303C ADSL construct.

■ ABBREVIATIONS

ADSL, adenylosuccinate lyase; WT, wild type; SAICAR, succinylaminoimidazolecarboxamide ribonucleotide; AICAR, aminoimidazolecarboxamide ribotide; SAMP, succinyladenosine monophosphate; AMP, adenosine monophosphate; PMR, psychomotor retardation; SAICAr, succinylaminoimidazolecarboxamide riboside; S-Ado, succinyladenosine; DTT, DL-dithiothreitol; EDTA, ethylenediaminetetraacetic acid tetrasodium salt dihydrate; Ap, ampicillin; ITC, isothermal titration calorimetry; HEPES, *N*-(2-hydroxyethyl)piperazine-*N*′-2-ethanesulfonate; IPTG, isopropyl β-D-thiogalactoside; LB, Luria-Bertani; NCBI, National Center for Biotechnology Information; PEG, polyethylene glycol; PPT, phenylpyruvate tautomerase; SDS−PAGE, sodium dodecyl sulfate−polyacrylamide gel electrophoresis; Tris, tris(hydroxymethyl)aminomethane.

■ REFERENCES

(1) Spiegel, E. K., Colman, R. F., and Patterson, D. (2006) Adenylosuccinate lyase deficiency. *Mol. Genet. Metab. 89*, 19−31.

(2) Mouchegh, K., Zikanova, M., Hoffmann, G. F., Kretzschmar, B., Kuhn, T., Mildenberger, E., Stoltenburg-Didinger, G., Krijt, J., Dvorakova, L., Honzik, T., Zeman, J., Kmoch, S., and Rossi, R.

(2007) Lethal fetal and early neonatal presentation of adenylosuccinate lyase deficiency: Observation of 6 patients in 4 families. *J. Pediatr. 150*, 57−61.
(3) Gitiaux, C., Ceballos-Picot, I., Marie, S., Valayannopoulos, V., Rio, M., Verrieres, S., Benoist, J. F., Vincent, M. F., Desguerre, I., and Bahi-Buisson, N. (2009) Misleading behavioural phenotype with adenylosuccinate lyase deficiency. *Eur. J. Hum. Genet. 17*, 133−136.
(4) Kohler, M., Assmann, B., Brautigam, C., Storm, W., Marie, S., Vincent, M.-F., Berghe, G. V. D., Simmonds, H. A., and Hoffmann, G. F. (1999) Adenylosuccinase Deficiency: Possibly Underdiagnosed Encephalopathy with Variable Clinical Features. *Eur. J. Paediatr. Neurol. 3*, 3−6.
(5) Jurecka, A., Zikanova, M., Tylki-Szymanska, A., Krijt, J., Bogdanska, A., Gradowska, W., Mullerova, K., Sykut-Cegielska, J., Kmoch, S., and Pronicka, E. (2008) Clinical, biochemical and molecular findings in seven Polish patients with adenylosuccinate lyase deficiency. *Mol. Genet. Metab. 94*, 435−442.
(6) Ciardo, F., Salerno, C., and Curatolo, P. (2001) Neurologic aspects of adenylosuccinate lyase deficiency. *Journal of Child Neurology 16*, 301−308.
(7) Jaeken, J., and Vandenberghe, G. (1984) An Infantile Autistic Syndrome Characterized by the Presence of Succinyl Purines in Body-Fluids. *Lancet 2*, 1058−1061.
(8) Vandenbergh, F., Vincent, M. F., Jaeken, J., and Vandenberghe, G. (1993) Residual Adenylosuccinase Activities in Fibroblasts of Adenylosuccinase-Deficient Children: Parallel Deficiency with Adenylosuccinate and Succinyl-Aicar in Profoundly Retarded Patients and Nonparallel Deficiency in a Mildly Retarded Girl. *J. Inherited Metab. Dis. 16*, 415−424.
(9) Sivendran, S., and Colman, R. F. (2008) Effect of a new non-cleavable substrate analog on wild-type and serine mutants in the signature sequence of adenylosuccinate lyase of *Bacillus subtilis* and *Homo sapiens*. *Protein Sci. 17*, 1162−1174.
(10) Hurlimann, H. C., Laloo, B., Simon-Kayser, B., Saint-Marc, C., Coulpier, F., Lemoine, S., Daignan-Fornier, B., and Pinson, B. (2011) Physiological and Toxic Effects of Purine Intermediate 5-Amino-4-imidazolecarboxamide Ribonucleotide (AICAR) in Yeast. *J. Biol. Chem. 286*, 30994−31002.
(11) Baresova, V., Skopova, V., Sikora, J., Patterson, D., Sovova, J., Zikanova, M., and Kmoch, S. (2012) Mutations of ATIC and ADSL affect purinosome assembly in cultured skin fibroblasts from patients with AICA-ribosiduria and ADSL deficiency. *Hum. Mol. Genet. 21*, 1534−1543.
(12) Lundy, C. T., Jungbluth, H., Pohl, K. R. E., Siddiqui, A., Marinaki, A. M., Mundy, H., and Champion, M. P. (2010) Adenylosuccinate Lyase Deficiency in the United Kingdom Pediatric Population: First Three Cases. *Pediatric Neurology 43*, 351−354.
(13) Race, V., Marie, S., Vincent, M. F., and Van den Berghe, G. (2000) Clinical, biochemical and molecular genetic correlations in adenylosuccinate lyase deficiency. *Hum. Mol. Genet. 9*, 2159−2165.
(14) Zikanova, M., Skopova, V., Hnizda, A., Krijt, J., and Kmoch, S. (2010) Biochemical and Structural Analysis of 14 Mutant ADSL Enzyme Complexes and Correlation to Phenotypic Heterogeneity of Adenylosuccinate Lyase Deficiency. *Hum. Mutat. 31*, 445−455.
(15) Toth, E. A., Worby, C., Dixon, J. E., Goedken, E. R., Marqusee, S., and Yeates, T. O. (2000) The crystal structure of adenylosuccinate lyase from *Pyrobaculum aerophilum* reveals an intracellular protein with three disulfide bonds. *J. Mol. Biol. 301*, 433−450.
(16) Tsai, M., Koo, J., Yip, P., Colman, R. F., Segal, M. L., and Howell, L. (2007) Substrate and product complexes of *Escherichia coli* adenylosuccinate lyase provide new insights into the enzymatic mechanism. *J. Mol. Biol. 370*, 541−554.
(17) Brosius, J. L., and Colman, R. F. (2002) Three subunits contribute amino acids to the active site of tetrameric adenylosuccinate lyase: Lys(268) and Glu(275) are required. *Biochemistry 41*, 2217−2226.
(18) Sivendran, S., Patterson, D., Spiegel, E., McGown, I., Cowley, D., and Colman, R. F. (2004) Two novel mutant human adenylosuccinate lyases (ASLs) associated with autism and characterization of the equivalent mutant *Bacillus subtilis* ASL. *J. Biol. Chem. 279*, 53789−53797.
(19) Palenchar, J. B., and Colman, R. F. (2003) Characterization of a mutant *Bacillus subtilis* adenylosuccinate lyase equivalent to a mutant enzyme found in human adenylosuccinate lyase deficiency: Asparagine 276 plays an important structural role. *Biochemistry 42*, 1831−1841.
(20) Ariyananda, L. D., Lee, P., Antonopoulos, C., and Colman, R. F. (2009) Biochemical and Biophysical Analysis of Five Disease-Associated Human Adenylosuccinate Lyase Mutants. *Biochemistry 48*, 5291−5302.
(21) Ariyananda, L. D., Antonopoulos, C., Currier, J., and Colman, R. F. (2011) In Vitro Hybridization and Separation of Hybrids of Human Adenylosuccinate Lyase from Wild-Type and Disease-Associated Mutant Enzymes. *Biochemistry 50*, 1336−1346.
(22) Race, V., Marie, S., Vincent, M. F., and Van den Berghe, G. (2000) Clinical, biochemical and molecular genetic correlations in adenylosuccinate lyase deficiency. *Hum. Mol. Genet. 9*, 2159−2165.
(23) Kmoch, S., Hartmannova, H., Stiburkova, B., Krijt, J., Zikanova, M., and Sebesta, I. (2000) Human adenylosuccinate lyase (ADSL), cloning and characterization of full-length cDNA and its isoform, gene structure and molecular basis for ADSL deficiency in six patients. *Hum. Mol. Genet. 9*, 1501−1513.
(24) Zikanova, M., Krijt, J., Hartmannova, H., and Kmoch, S. (2005) Preparation of 5-amino-4-imidazole-N-succinocarboxamide ribotide, 5-amino-4-imidazole-N-succinocarboxamide riboside and succinyladenosine, compounds usable in diagnosis and research of adenylosuccinate lyase deficiency. *J. Inherited Metab. Dis. 28*, 493−499.
(25) Gill, S., and von Hippel, P. (1989) Calculation of protein extinction coefficients from amino acid sequence data. *Anal. Biochem. 182*, 319−326.
(26) Lee, P., and Colman, R. F. (2007) Expression, purification, and characterization of stable, recombinant human adenylosuccinate lyase. *Protein Expression Purif. 51*, 227−234.
(27) Collaborative Computational Project, Number 4 (1994) The CCP4 suite: Programs for protein crystallography. *Acta Crystallogr. D50*, 760−763.
(28) Mccoy, A. J., Grosse-Kunstleve, R. W., Adams, P. D., Winn, M. D., Storoni, L. C., and Read, R. J. (2007) Phaser crystallographic software. *J. Appl. Crystallogr. 40*, 658−674.
(29) Emsley, P., and Cowtan, K. (2004) Coot: Model-building tools for molecular graphics. *Acta Crystallogr. D60*, 2126−2132.
(30) Murshudov, G. N., Vagin, A. A., and Dodson, E. J. (1997) Refinement of macromolecular structures by the maximum-likelihood method. *Acta Crystallogr. D53*, 240−255.
(31) Pearlman, D. A., Case, D. A., Caldwell, J. W., Ross, W. S., Cheatham, T. E., Debolt, S., Ferguson, D., Seibel, G., and Kollman, P. (1995) Amber, a Package of Computer-Programs for Applying Molecular Mechanics, Normal-Mode Analysis, Molecular-Dynamics and Free-Energy Calculations to Simulate the Structural and Energetic Properties of Molecules. *Comput. Phys. Commun. 91*, 1−41.
(32) Case, D. A., Cheatham, T. E., Darden, T., Gohlke, H., Luo, R., Merz, K. M., Onufriev, A., Simmerling, C., Wang, B., and Woods, R. J. (2005) The Amber biomolecular simulation programs. *J. Comput. Chem. 26*, 1668−1688.
(33) Jorgensen, W. L., Chandrasekhar, J., Madura, J. D., Impey, R. W., and Klein, M. L. (1983) Comparison of Simple Potential Functions for Simulating Liquid Water. *J. Chem. Phys. 79*, 926−935.
(34) Hornak, V., Abel, R., Okur, A., Strockbine, B., Roitberg, A., and Simmerling, C. (2006) Comparison of multiple Amber force fields and development of improved protein backbone parameters. *Proteins: Struct., Funct., Bioinf. 65*, 712−725.
(35) Vandenbergh, F., Vincent, M. F., Jaeken, J., and Vandenberghe, G. (1993) Functional Studies in Fibroblasts of Adenylosuccinase-Deficient Children. *J. Inherited Metab. Dis. 16*, 425−434.
(36) Toth, E. A., and Yeates, T. O. (2000) The structure of adenylosuccinate lyase, an enzyme with dual activity in the de novo purine biosynthetic pathway. *Struct. Folding Des. 8*, 163−174.